Matter Power Spectrum Covariance Matrix from the DEUS-PUR ΛCDM simulations: Mass Resolution and non-Gaussian Errors

L Blot, P. Corasaniti, Jean-Michel Alimi, V Reverdy, Y Rasera

Matter Power Spectrum Covariance Matrix from the DEUS-PUR ΛCDM simulations: Mass Resolution and non-Gaussian Errors

L. Blot[1][*], P.S. Corasaniti[1], J.-M. Alimi[1,2], V. Reverdy[1], Y. Rasera[1]

[1]*Laboratoire Univers et Théories, UMR 8102 CNRS, Observatoire de Paris, Université Paris Diderot, 5 Place Jules Janssen, 92190 Meudon, France*
[2]*Institut d'Astrophysique, UMR 7095 CNRS, Université Pierre et Marie Curie, 98bis Blvd Arago, 75014 Paris, France*

14 June 2018

ABSTRACT
The upcoming generation of galaxy surveys will probe the distribution of matter in the universe with unprecedented accuracy. Measurements of the matter power spectrum at different scales and redshifts will provide stringent constraints on the cosmological parameters. However, on non-linear scales this will require an accurate evaluation of the covariance matrix. Here, we compute the covariance matrix of the 3D matter density power spectrum for the concordance ΛCDM cosmology from an ensemble of N-body simulations of the Dark Energy Universe Simulation - Parallel Universe Runs (DEUS-PUR). This consists of 12288 realisations of a $(656\,h^{-1}\,\mathrm{Mpc})^3$ simulation box with 256^3 particles. We combine this set with an auxiliary sample of 96 simulations of the same volume with 1024^3 particles. We find N-body mass resolution effect to be an important source of systematic errors on the covariance at high redshift and small intermediate scales. We correct for this effect by introducing an empirical statistical method which provide an accurate determination of the covariance matrix over a wide range of scales including the Baryon Oscillations interval. Contrary to previous studies that used smaller N-body ensembles, we find the power spectrum distribution to significantly deviate from expectations of a Gaussian random density field at $k \gtrsim 0.25\,h\,\mathrm{Mpc}^{-1}$ and $z < 0.5$. This suggests that in the case of finite volume surveys an unbiased estimate of the ensemble averaged band power at these scales and redshifts may require a careful assessment of non-Gaussian errors more than previously considered.

Key words: Cosmology: dark matter - Methods: N-body simulations

1 INTRODUCTION

Surveys of the large scale structures have been providing insightful data for more than a decade now. Observational projects such as the 2-degree Field Galaxy Redshift Survey (2dFGRS, Percival et al. 2001; Cole et al. 2005) and the Sloan Digital Sky Survey (SDSS, Tegmark et al. 2004) have yielded unprecedented measurements of the clustering of matter on the large scales. These observations have made possible the first detection of the Baryon Acoustic Oscillations (BAO) signal (Eisenstein et al. 2005; Percival et al. 2007) and provided constraints on model parameters that are complementary to those obtained from other standard cosmological probes. The success of these projects has opened the way to a new generation of survey programs.

In the years to come the Dark Energy Survey[1] (DES), the Large Synoptic Survey Telescope[2] (LSST) or the Euclid mission[3] will map the distribution of galaxies in larger cosmic volumes and

with higher sensitivity. Through a variety of probes, these surveys aim to achieve a few percent error on the determination of several cosmological parameters. However, multiple challenges need to be addressed. From the theoretical point of view one of the most challenging aspects concerns the availability of robust theoretical predictions of the clustering of matter at small scales, which is crucial to correctly interpret the data and infer unbiased constraints on model parameters.

At small scales and late times the gravitational collapse becomes a highly non-linear process. Thus, model predictions cannot rely on standard linear perturbation theory and require solving the complex dynamics of matter collapse through numerical simulations. The need for accurate predictions of the clustering of matter over large interval of scales has driven up the demand for large volume high-resolution N-body simulations (Angulo et al. 2012; Kim et al. 2011; Alimi et al. 2012; Skillman et al. 2014). As an example the Baryon Oscillation Spectroscopic Survey (BOSS, Dawson et al. 2013) has recently determined the cosmic distance scale to one percent accuracy from measurements of the BAO spectrum in the range of modes $0.01 < k[\,h\,\mathrm{Mpc}^{-1}] < 0.30$ (Anderson et al. 2013). Future surveys such as LSST or Euclid will push these measurements even further by probing the cluster-

---

[1] www.darkenergysurvey.org
[2] www.lsst.org
[3] www.euclid-ec.org

ing of matter up to $k \approx 1 \, h \, \mathrm{Mpc}^{-1}$ (see e.g. Abell et al. 2009; Amendola et al. 2012). Predicting the matter power spectrum in such a large interval of scales at a few percent level is a very challenging task since it requires N-body simulations that cover very large cosmic volumes to reduce cosmic variance uncertainties at low k and with sufficient mass and spatial resolution to limit numerical systematic errors at large k. To tackle this challenge Alimi et al. (2012) have realised a series of N-body simulations, the Dark Energy Universe Simulation Full Universe Runs (DEUS-FUR), covering a cosmic volume of $(21 \, \mathrm{Gpc} \, h^{-1})^3$ with 8192^3 particles which has allowed to resolve the BAO spectrum to 1% accuracy level (Rasera et al. 2014). However, this is still not sufficient to correctly interpret the data since an unbiased statistical analysis also require knowledge of the covariance matrix. Addressing this issue is the goal of the analysis presented here.

If the initial matter density field is Gaussian distributed, during the linear regime its Fourier modes evolve independently and the covariance of the matter power spectrum has a simple diagonal form. From now on we will refer to this configuration as the Gaussian case, for which errors on the band powers are uncorrelated. In contrast at small scales and late times the covariance develops non-vanishing off-diagonal terms which account for the mode coupling caused by the non-linear regime of gravitational collapse. In such a case the errors on band powers become correlated causing a larger dispersion on power spectrum measurements (Meiksin & White 1999). Neglecting such correlations may lead to biased results as shown by several studies of weak lensing observables (see e.g. White & Hu 2000; Semboloni et al. 2007; Lee & Pen 2008; Kiessling, Taylor & Heavens 2011) and to a biased determination of BAO parameters (see e.g. Takahashi et al. 2011; Ngan et al. 2012). Hence, the future generation of large scale structure surveys will need estimates of the covariance matrix which require sampling the matter power spectrum from large samples of N-body simulations (Taylor, Joachimi & Kitching 2013).

We undertake this task using a set of simulations ($\sim 10^4$) of the concordance ΛCDM model from the Dark Energy Universe Simulation Parallel Universe Runs (DEUS-PUR). By combining this large ensemble with an auxiliary set of high resolution runs we estimate the impact of the mass resolution of the simulations on the 3D matter density power spectrum covariance matrix. We show that mass resolution effects can be an important source of uncertainty. Furthermore, our analysis clearly indicates the necessity of using large N-body datasets when studying the matter power spectrum distribution at small scales and low redshifts. In particular we find significant deviations from expectations of a Gaussian density field which were overlooked in previous studies. This has potentially important implications for inferring unbiased power spectrum measurements for future survey programs. Our work extends the analysis of Takahashi et al. (2009) to a larger statistical sample of N-body simulations with higher mass resolution and better spatial resolution.

The paper is organised as follows: in Section 2 we describe the characteristics of the DEUS-PUR simulations. In Section 3 we present the analysis of the DEUS-PUR covariance matrix, while in Section 4 we show the results of the computation of the probability distribution of the matter power spectrum. In Section 5 we discuss the effect of non-Gaussian errors on the signal-to-noise of power spectrum measurement. Finally we present our conclusion in Section 6.

h	$\Omega_m h^2$	$\Omega_b h^2$	n_s	σ_8
0.72	0.1334	0.02258	0.963	0.801

Table 1. DEUS-PUR cosmological model parameter values.

2   N-BODY DATASET

2.1   DEUS-PUR Simulations

We use the N-body simulation dataset from DEUS-PUR project. This consists of 12288 simulations of a flat ΛCDM model with parameters (see Table 1) calibrated to the WMAP-7yr data (Spergel et al. 2007) of a cosmological volume of $(656 \, h^{-1} \, \mathrm{Mpc})^3$ with 256^3 particles, for a formal mass resolution of $1.2 \times 10^{12} \, h^{-1} \, \mathrm{M}_\odot$ (Set A), and 96 simulations of the same cosmological model and equal volume with 1024^3 particles, corresponding to a mass resolution of $2 \times 10^{10} \, h^{-1} \, \mathrm{M}_\odot$ (Set B). These runs have been realised with "A Multiple purpose Application for Dark Energy Universe Simulation" (AMADEUS) (Alimi et al. 2012). This workflow application includes a dynamical solver based on RAMSES (Teyssier 2002), an adaptive mesh refinement code with a tree-based data structure that allows recursive grid refinement on a cell-by-cell basis, in which particles are evolved using a particle-mesh (PM) solver, while the Poisson equation is solved using a multigrid method (Guillet & Teyssier 2011). In the case of the DEUS-PUR simulations the refinement criterion is set such as to allow up to 6 levels of refinement.

The initial conditions of the simulations have been generated using the code MPGRAFIC (Prunet et al. 2008), which convolves a white noise with the square root of the input power spectrum and generates initial displacements and velocities of the dark matter particles using the Zeldovich approximation. In order to avoid the generation of $\sim 10^4$ white noises we generated 3 independent white noises in 3 cubes of 4096^3 particles each that we have subsequently split into 4096 sub-cubes. The latter were then used separately to generate the initial conditions of each simulation of Set A. A similar procedure has been used to generate the initial conditions of the simulations of Set B. These have been obtained by splitting 2 different white noises of 4096^3 particles in 64 cubes. The initial redshift has been set such that all simulations starts with the same amplitude of density fluctuations at the scale of the grid resolution. This is a standard technique that allows to consistently compare simulations with different spatial and mass resolution. Let us denote by $\sigma(L/N_p, z_i)$ the root-mean-square fluctuation of the linear density field at an initial redshift z_i on the scale of the grid resolution L/N_p, where L is the simulation box-length and N_p is the number of particles. Then, z_i is determined by setting $\sigma(L/N_p, z_i)$ to an arbitrary small value and iteratively solving the algebraic equation

$$\frac{\sigma(L/N_p, z_i)}{\sigma(L/N_p, z = 0)} = \frac{D_+(z_i)}{D + (z = 0)}, \tag{1}$$

where D_+ is the linear growth function. We set $\sigma(L/N_p, z_i) = 0.02$, such that initial redshifts are sufficiently large to ensure the validity of the Zeldovich approximation, but not exceedingly large such as to avoid the introduction of systematic effects due to integration of numerical noise. In the case of simulation Set A this gives $z_i \approx 105$, while for the higher resolution Set B we have $z_i \approx 190$. Such large values guarantee that transient effects (Scoccimarro 1998; Crocce et al. 2006) are negligible. Table 2 summarises the characteristics of the DEUS-PUR simulations.

Set	N_s	L (Mpc h^{-1})	N_p	m_p ($M_\odot$ h^{-1})
A	12288	656.25	256^3	1.2×10^{12}
B	96	656.25	1024^3	2×10^{10}

Table 2. DEUS-PUR simulation characteristics: N_s is the number of realisations, L is the box-side length, N_p is the number of dark matter particles and m_p the mass resolution. Taking set A as a reference, set B has been designed to study simulation mass resolution effects on large scale structure observables.

Takahashi et al. (2009) have performed a study of the 3D power spectrum covariance matrix from 5000 simulations of a standard ΛCDM model with a $(1000\,h^{-1}\,\mathrm{Mpc})^3$ volume and a mass resolution of $4.1 \times 10^{12}\,h^{-1}\,\mathrm{M_\odot}$, realised with a Particle Mesh (PM) solver with no spatial refinement and initial redshift $z_i = 20$. For comparison our Set A has nearly 3 times more realisations which allow us to determine the covariance matrix with reduced statistical errors. Furthermore, the DEUS-PUR simulations have a mass resolution ~ 3 times higher, a better spatial resolution at the level of the coarse grid by nearly a factor of 1.5 (and a factor of ~ 100 at the most refined level) and start at a much higher redshift, thus allowing us to reduce the effect of numerical systematics when compared to the sample used by Takahashi et al. (2009).

The workflow of the AMADEUS application has been automated to generate a large number of N-body simulations. An external script has been coded to monitor in real time the job-queue and submit new simulations as soon as other simulations have terminated. For each simulation the initial conditions, the dynamic evolution, the data reduction and measurements of the matter power spectrum and the halo mass function are controlled through the same script. A final check on the file content has been implemented to detect any error due to unexpected machine failure. Each AMADEUS script has been launched as a separate job on the ADA supercomputer [4] of the Institute for Development and Resources in Intensive Scientific Computing (IDRIS). Simulations of Set A were run on 8 processors Intel Sandy Bridge E5-4650 for a running time of ~ 1 hour per simulation, while Set B simulations took ~ 24 hours per simulation on 64 processors.

2.2 Power Spectrum & Covariance Matrix Estimators

We compute the matter power spectrum using the code POWER-GRID (Prunet et al. 2008). This estimates the power spectrum from the Fourier transform of the matter density field in band powers of size $\Delta k = 2\pi/L$. We correct the measured spectrum for the effect of smoothing due to the Could-In-Cell (CIC) algorithm, that is used to estimate the density contrast field from the particle distribution. We do not correct for aliasing, since varying the size of the CIC grid we find that aliasing effects are negligible below half the Nyquist frequency of the CIC grid. Since our CIC grid is two times finer than the coarse grid of the simulation, its Nyquist frequency is given by $k_N = 2\left(\sqrt[3]{N_p}\,\pi/L\right)$. Thus the range of modes in which we compute the power spectrum is given by $k_{\min} = 2\pi/L$ and $k_{\max} = k_N/2$. More specifically $k_{\min} \approx 0.01\,h\,\mathrm{Mpc}^{-1}$ for both sets A and B, while $k_{\max} \approx 1.22\,h\,\mathrm{Mpc}^{-1}$ for set A and $k_{\max} \approx 5.9\,h\,\mathrm{Mpc}^{-1}$ for set B. To be conservative we restrict our analysis to Fourier modes up to $k \approx 1\,h\,\mathrm{Mpc}^{-1}$.

The covariance matrix is computed using the unbiased sample covariance estimator:

$$\widehat{\mathrm{cov}}(k_1, k_2) = \frac{1}{N_s - 1} \sum_{i=1}^{N_s} [\hat{P}_i(k_1) - \bar{P}(k_1)][\hat{P}_i(k_2) - \bar{P}(k_2)], \tag{2}$$

where N_s is the number of independent realisations and $\bar{P}(k) = \sum_{i=1}^{N_s} \hat{P}_i(k)/N_s$ is the sample mean, with $\hat{P}_i(k)$ the matter power spectrum estimation of the i-th realisation.

3 DEUS-PUR COVARIANCE MATRIX

Let us consider the formal expression of the matter power spectrum covariance matrix (see e.g. Scoccimarro, Zaldarriaga & Hui 1999):

$$\mathrm{cov}(k_1, k_2) = \frac{2}{N_{k_1}} P^2(k_1)\delta_{k_1, k_2} + \\ + \frac{1}{V} \int_{\Delta_{k_1}} \int_{\Delta_{k_2}} \frac{d^3\mathbf{k_1'}}{V_{k_1}} \frac{d^3\mathbf{k_2'}}{V_{k_2}} T(\mathbf{k_1'}, -\mathbf{k_1'}, \mathbf{k_2'}, -\mathbf{k_2'}), \tag{3}$$

where $P(k)$ is the matter power spectrum, $N_k \approx k^2 \Delta k\, V/(2\pi^2)$ is the number of k-modes in the volume V, Δ_{k_i} is the band power integration interval centred on the mode k_i and V_{k_i} is the integration volume in Fourier space; the integrand $T(\mathbf{k_1'}, \mathbf{k_2'}, \mathbf{k_3'}, \mathbf{k_4'})$ is the trispectrum (the fourth order connected moment in Fourier space) of the density fluctuation field. The first term in Eq. (3) represents the Gaussian contribution to the covariance. As already mentioned, for an initial Gaussian density field, during the linear regime the Fourier modes evolve independently and the power spectrum covariance is diagonal with amplitude $2P^2(k)/N_k$. The second term in Eq. (3) represents the contribution of non-Gaussianity arising during the non-linear regime of gravitational collapse at small scales.

Non-linearities induce mode couplings which source a non-vanishing trispectrum of the density fluctuation field. Since this cannot be computed exactly then the covariance matrix must be estimated by sampling the matter power spectrum from a large ensemble of numerical N-body simulations. This computation is not exempt of systematic uncertainties. For instance, the finite volume of simulations is source of non-Gaussian errors (Rimes & Hamilton 2006) and as shown in Takahashi et al. (2009) this can introduce large uncertainties even on weakly non-linear scales. We leave a detailed study of this effect to a forthcoming work. In the following, we focus on systematic errors due to the mass resolution of the simulations, which have been neglected in previous studies.

3.1 Numerical Simulation Mass Resolution Errors

In the top panel of Fig. 1 we plot the diagonal elements of the matter power spectrum covariance matrix normalised to the linear Gaussian amplitude $2\,P_{lin}^2(k)/N_k$ for Set A (dash lines) and B (solid lines) at $z = 0, 0.3, 0.5, 1$ and 2 (top to bottom) respectively. As we can see the curves corresponding to Set A are very smooth since they have negligible noise due to the large size of the simulation sample. This is not the case of Set B for which the covariance estimates are characterised by a higher level of noise. As expected, the onset of the non-linear regime causes deviations from the Gaussian prediction which occur at large k-values and shift towards smaller ones at lower redshifts. For instance, a deviation of a factor ~ 5 at $z = 1$ occurs at $k \sim 0.55\,h\,\mathrm{Mpc}^{-1}$, while at $z = 0$ the same deviation occurs at $k \sim 0.30\,h\,\mathrm{Mpc}^{-1}$. The effect of such deviations
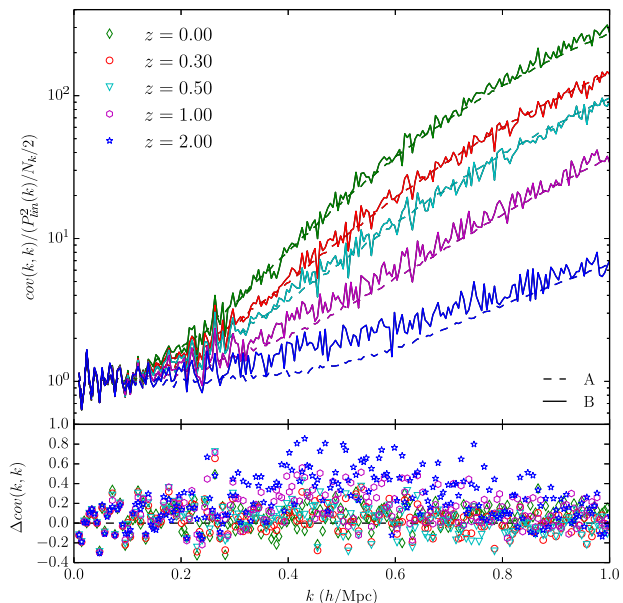
Figure 1. Top panel: diagonal elements of the covariance matrix normalised to the Gaussian variance for Set A (dashed lines) and B (solid lines) at $z = 0$ (green), 0.3 (red), 0.5 (light-blue), 1 (magenta) and 2 (blue) respectively. Bottom panel: relative difference between Set A and B at different redshifts. The variance of Set A is underestimated compared to that of Set B.

Figure 2. Top panel: as in Fig. 1 including the diagonal components of the covariance matrix from the corrected spectra of Set A (dot-dashed line). Middle panel: relative difference of the uncorrected variance of Set A (central) with respect to the corrected one. Corrections can be as large as 40 per cent at $z = 2$, 20 per cent at $z = 1$ and less than 10 per cent at lower redshifts. Bottom panel: relative difference of the variance from the higher resolution simulations Set B with respect to the correct variance. The residuals show no systematic shift indicating that the correction efficiently accounts for the mass resolution effect.

is to increase the statistical errors on the power spectrum measurements at non-linear scales. Despite the higher level of statistical noise associated to Set B, it is evident that there is a systematic down shift of the variance of lower resolution simulations. In the bottom panel of Fig. 1 we can see that such a discrepancy exceeds the statistical noise of Set B at redshifts $z > 0.5$ in the range of modes $0.20 \lesssim k [\, h \, \mathrm{Mpc}^{-1}] \lesssim 0.80$ with an amplitude that on average can be as large as ~ 40 per cent. This is a direct consequence of the suppression of the matter power spectrum at large/intermediate k for lower mass resolution simulations.

The mass resolution of numerical simulations is a known source of systematic errors and a generic feature of simulations which rely on the PM method (Joyce et al. 2009; Heitmann et al. 2010; Rasera et al. 2014). The suppression of power at small scales for lower mass resolution simulations is due to the combination of the precision of force calculation, which is based on grid discretization of the gravitational field, and the particle sampling of the matter density field. In a PM code the number of coarse grids is usually set equal to the number of particles, therefore, before any refinement is triggered, particles in under-dense or over-dense regions will experience a reduced force by the close environment compared to higher resolution simulations. Knebe et al. (2001) showed that for PM based codes the ideal configuration is to have 8 times more grid points than particles, but in a cosmological simulation this requirement may be too expensive from the computational point of view. None the less, the artificial suppression of power is mitigated at low redshifts and/or higher k when the local density of particles in the simulations triggers the AMR grid refinement, which explains why this systematic effect shown in Fig. 1 fades away across the whole interval at $z \leq 0.5$.

Rasera et al. (2014) corrected the BAO spectrum for the mass resolution effect by combining the cosmic variance limited power spectrum from DEUS-FUR wi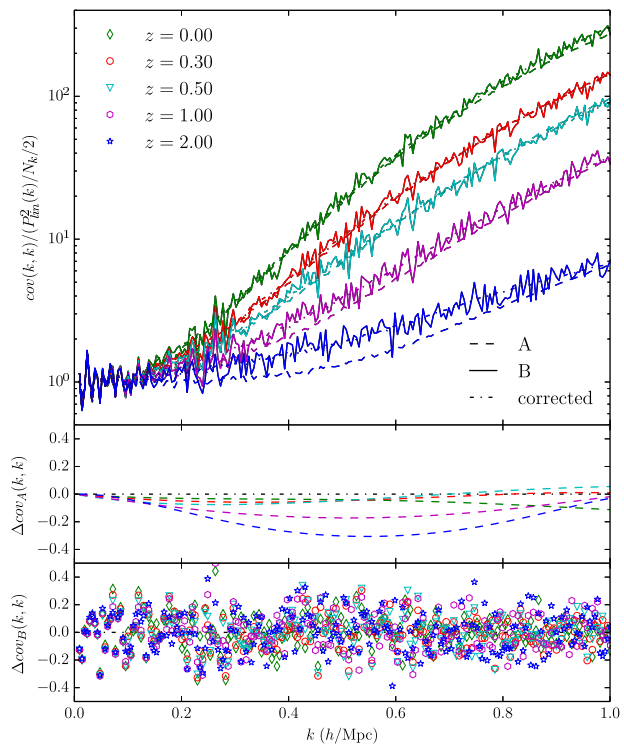th that of smaller volume and higher resolution simulations. Here, we opt for a similar strategy. In fact, the covariance is obtained by sampling the matter power spectrum of independent realisations, thus we can correct the lower resolution power spectra of Set A by implementing statistical information on the power spectra obtained from the higher resolution simulations of Set B. In Appendix A we provide a detailed derivation of the correction, which we assume to be linear:

$$\hat{P}_{\mathrm{A}}^{\mathrm{corr}}(k) = \left[\hat{P}_{\mathrm{A}}(k) - \bar{P}_{\mathrm{A}}(k) \right] \frac{\sigma_{\hat{P}_{\mathrm{B}}}(k)}{\sigma_{\hat{P}_{\mathrm{A}}}(k)} + \bar{P}_{\mathrm{B}}(k), \qquad (4)$$

where $\bar{P}_{\alpha}(k)$ and $\sigma_{P_{\alpha}}(k)$ ($\alpha = \mathrm{A}, \mathrm{B}$) are the average and root-mean-square of the power spectrum estimator respectively.

In Fig. 2 we show the diagonal elements of the covariance matrix normalised to the Gaussian term for Set A before (dash lines) and after (dash dot lines) correction, and for set B (solid lines) at $z = 0.0, 0.3, 0.5, 1.0$ and 2.0 (top to bottom) respectively. As we can see the corrected curves fit well through those obtained from the higher resolution simulations. In the middle panel of Fig. 2 we show the relative differences between the corrected and uncorrected curves at different redshifts (dash lines top to bottom corresponds to $z = 0$ to 2). We can clearly see that the amplitude of the correction at high redshift in the interval $0.20 \lesssim k [\, h \, \mathrm{Mpc}^{-1}] \lesssim 0.80$ can be as large as 40 per cent, while at $z < 0.5$ the difference remains below the 10 per cent level. In the bottom panel of Fig. 2 we also plot the residual between the corrected covariance of Set A and that

from Set B (different dot types correspond to different redshifts as shown in the legend). As we can see there is no systematic shift and the only differences are due to the statistical noise of Set B.

The mass resolution error also underestimate the off-diagonal components of the covariance matrix, none the less the amplitude results to be smaller than the systematic shift we have seen on the diagonal elements. As expected we find the correction of the low resolution power spectra to also account for the mass resolution effect on the off-diagonal components.

3.2 Fourier Mode Correlations

In order to quantify the correlation between pairs of Fourier modes it is useful to introduce the correlation coefficient

$$r(k_1, k_2) = \frac{\mathrm{cov}(k_1, k_2)}{\sqrt{\mathrm{cov}(k_1, k_1)\,\mathrm{cov}(k_2, k_2)}}, \quad (5)$$

which varies between 1 (maximum correlation) and -1 (maximum anti-correlation), and is 0 when modes are uncorrelated. In linear regime the correlation coefficient is the identity matrix.

In Fig. 3 we plot $r(k_1, k_2)$ in the interval $0.03 < k[\,h\,\mathrm{Mpc}^{-1}] < 1.00$ (which includes the BAO range) at $z = 2$ (left panels), 1 (central panels) and 0 (right panels) for Set A (top panels) and for Set B (bottom panels). We do not show the correlation coefficient inferred from the corrected spectra of Set A since this coincides with the uncorrected one to very good approximation. This is because the mass resolution effect discussed in the previous section scales approximately linearly with the power spectrum affecting the covariance matrix amplitude. Since correlation coefficient is given by the covariance matrix normalised by the root-square of the product of its diagonal elements the effect cancels out in the ratio.

Non-vanishing off-diagonal elements are already present at $z = 2$ at large k values, for instance the mode $k_1 \sim 0.3\,h\,\mathrm{Mpc}^{-1}$ has a 10 per cent correlation with $k_2 \sim 0.4\,h\,\mathrm{Mpc}^{-1}$ and 20 per cent with $k_2 \sim 1\,h\,\mathrm{Mpc}^{-1}$. The amplitude of the correlations increases as function of k and extends towards smaller k values at lower redshifts as the dynamics of the modes increasingly deviates from the linear regime of collapse. The comparison between the two sets shows the importance of having a large set of simulations, in order to reduce the impact of noise. In fact, the structure of correlations is much clearer for Set A than for Set B, for which at $z = 2$ the signal is hard to distinguish from the statistical noise. It is worth noticing that in the BAO range ($0.01 < k[\,h\,\mathrm{Mpc}^{-1}] < 0.30$) the correlation in the off-diagonal components can reach a level up to 30-35 per cent between redshift 1 and 0, which confirms the need of an accurate estimation of the 3D power spectrum covariance matrix for BAO data analyses.

4 PROBABILITY DISTRIBUTION OF THE POWER SPECTRUM

We now focus on the probability distribution function (PDF) of the matter power spectrum estimator.

In the case of Gaussian initial conditions, during the linear regime of gravitational collapse the matter power spectrum at a given wave-number k is distributed as a χ^2 with N_k degrees-of-freedom (see e.g. Fisher et al. 1993). In the large N_k limit, which corresponds to sufficiently large volumes and high wave-numbers, the PDF tends to a Gaussian. However, at high k the non-linear evolution of matter clustering is expected to introduce non-

Gaussianities (i.e. departures from a χ^2-distribution in the large N_k limit).

The large sample of simulations from DEUS-PUR allows us to finely sample such a distribution and test for non-Gaussianities. To this end it is convenient to rescale the power spectrum estimator as $\sqrt{N_k/2}(\hat{P}/\bar{P} - 1)$, such that in the large N_k limit and in linear regime the distribution is a Gaussian with zero mean and unity variance.

In Fig. 4 we plot the estimated PDF from Set A at $z = 0$ and $k = 0.05, 0.20, 0.40, 0.60$ and $1.00\,h\,\mathrm{Mpc}^{-1}$ respectively. The error bars are given by Poisson errors. At $k \leq 0.20\,h\,\mathrm{Mpc}^{-1}$ we can see that the PDF is consistent with a Gaussian distribution within statistical errors, while at higher k we can clearly see deviations from Gaussianity above statistical uncertainties. We quantify these deviations in terms of the skewness and kurtosis defined as:

$$S_3(k) = \frac{N_s^{-1} \sum_{i=1}^{N_s} [\hat{P}_i(k) - \bar{P}(k)]^3}{\left\{ N_s^{-1} \sum_{i=1}^{N_s} [\hat{P}_i(k) - \bar{P}(k)]^2 \right\}^{3/2}}, \quad (6)$$

$$S_4(k) = \frac{N_s^{-1} \sum_{i=1}^{N_s} [\hat{P}_i(k) - \bar{P}(k)]^4}{\left\{ N_s^{-1} \sum_{i=1}^{N_s} [\hat{P}_i(k) - \bar{P}(k)]^2 \right\}^2} - 3. \quad (7)$$

In the case of a χ^2-distribution with N_k degree-of-freedom these can be computed exactly resulting in $S_3(k) = \sqrt{8/N_k}$ and $S_4(k) = 12/N_k$ (see e.g. Takahashi et al. 2009).

In Fig. 5 we plot $S_3(k)$ (top panels) and $S_4(k)$ (bottom panels) from Set A estimated at $z = 105$ and $z = 0, 0.3, 0.5$ (where mass resolution effects are subdominant) respectively. For visual purposes we have binned the estimated values in bins of size $\Delta k/k = 0.1$ and included statistical errors on the data points. The dashed lines corresponds to the χ^2 expected values of $S_3(k)$ and $S_4(k)$. We notice that at $z = 105$ the skewness is consistent with that from the χ^2-distribution, while for $z < 0.5$ and $k \gtrsim 0.25\,h\,\mathrm{Mpc}^{-1}$ we can clearly see increasing deviations as function of k at high statistical significance. In contrast the kurtosis remains consistent with χ^2 expected values and any departure of $S_4(k)$ from the Gaussian random field prediction still remains within statistical errors.

Previous studies have determined the power spectrum distribution using smaller simulation ensembles and at low redshifts found no statistically significant deviation of the skewness from expectations of a Gaussian random density field (see e.g. Takahashi et al. 2009). This stresses the necessity of using very large samples of simulations. We believe that such a result can have important observational implications which warrant further investigation. At large k and $z < 0.5$ the ratio $S_3(k)/\sqrt{8/N_k} \gtrsim 2$, hence unbiased measurements of the band power from observables of the clustering of matter such as weak lensing observations (see also Sato et al. 2009) may require prior knowledge of the $\hat{P}(k)$ distribution. At lower k the departure from a χ^2-distribution is at most of a factor 2 for $k \lesssim 0.30\,h\,\mathrm{Mpc}^{-1}$. Thus, measurements of the BAO may still be performed using only covariance matrix information, though aiming at sub-percent accuracy may require a more detailed study to elucidate the full impact of the non-Gaussian distribution of $\hat{P}(k)$.

5 SIGNAL-TO-NOISE

We estimate the effect of the correlation between band power errors on the signal-to-noise of the matter power spectrum

$$\left(\frac{S}{N}\right)^2 = \sum_{k_1, k_2 < k_{\max}} P(k_1)\, \psi(k_1, k_2)\, P(k_2), \quad (8)$$
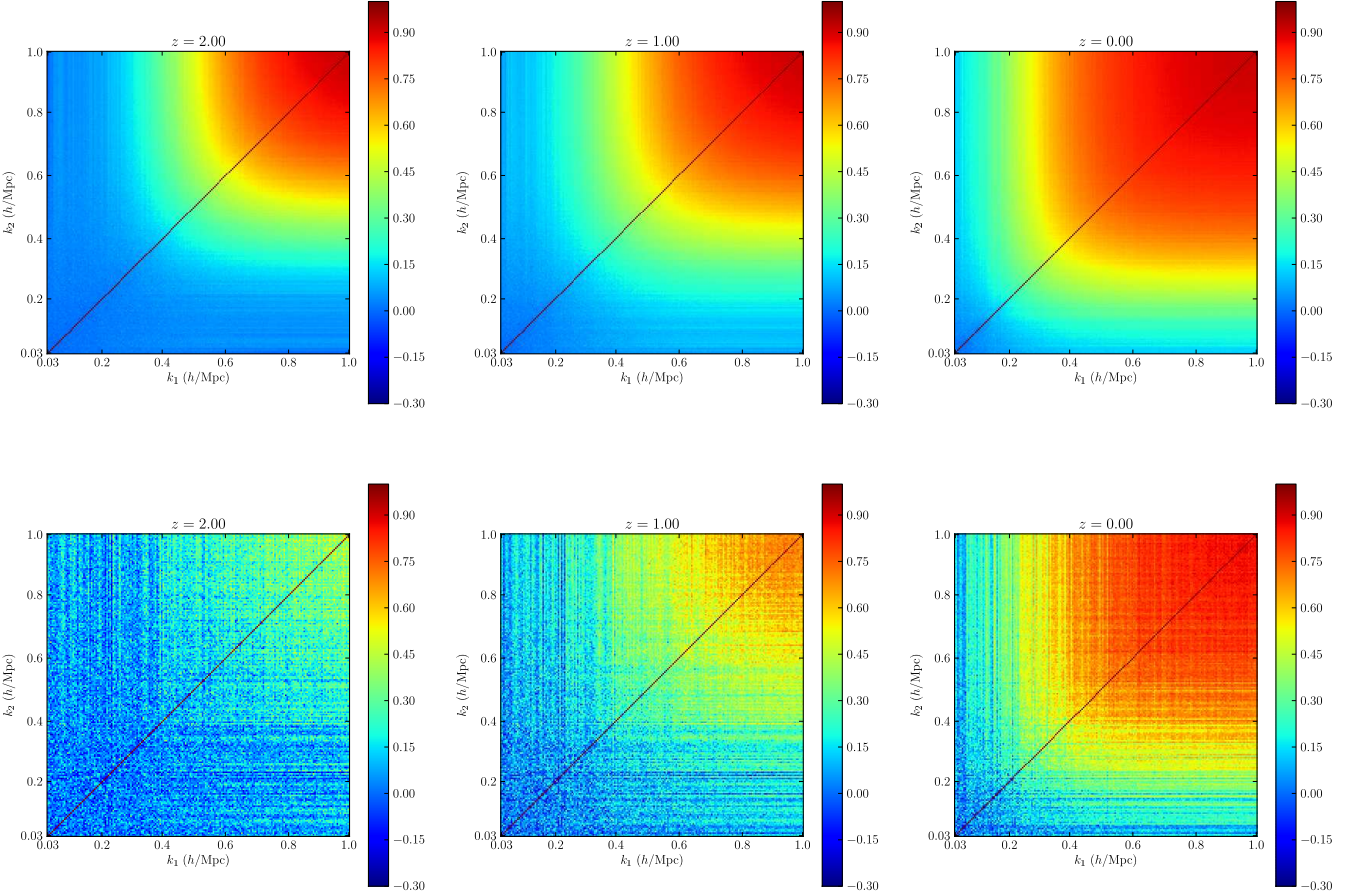
Figure 3. Correlation coefficient matrix at $z = 2$ (left panels), 1 (central panels) and 0 (right panels) respectively estimated from Set A (top panels) and Set B (bottom panels). We can see the increasing amplitude of pair correlation at high k shifting towards lower wave-numbers for decreasing redshift. The comparison between the two sets shows that the structure of the correlations is poorly reproduced when using a low number of simulations.

where $\psi = \mathrm{cov}^{-1}(k_1, k_2)$ is the inverse of covariance matrix, also known as precision matrix. Since we estimate the covariance from a finite ensemble of independent realisations, there is a statistical error associated to the sample covariance. Thus, inverting the sample covariance gives a biased estimate of the precision matrix. For a Gaussian random density field the unbiased estimator of the precision matrix is given by (see e.g. Hartlap, Simon & Schneider 2007; Taylor, Joachimi & Kitching 2013):

$$\widehat{\psi}(k_1, k_2) = \frac{N_s - N_b - 2}{N_s - 1}\, \widehat{\mathrm{cov}}^{-1}(k_1, k_2), \qquad (9)$$

where $\widehat{\mathrm{cov}}$ is the covariance estimator defined in Eq. (2), N_s is the number of realisations and N_b is the number of band power bins. This estimator is defined only for $N_s > N_b + 2$. In any case, for $N_s < N_b + 1$ the values of the sample covariance are not positive definite and its inverse is not defined (Hartlap, Simon & Schneider 2007).

In evaluating the signal-to-noise we set the power spectrum in Eq. (8) to the average of the corrected spectra from Set A and compute the signal-to-noise using the precision matrix defined by Eq. (9) for the corrected and uncorrected spectra of Set A respectively.

In Fig. 6 we plot the resulting signal-to-noise estimates at $z = 0, 0.3, 0.5, 1$ and 2 respectively as function of k_{max}. We can see that the effect of mass resolution errors is to artificially enhance the signal-to-noise. As discussed in Section 3.1 this is be-

cause lower mass resolution simulations underestimate the covariance matrix. This results into a greater amplitude of the precision matrix components and consequently in a larger signal-to-noise compared to higher mass resolution estimates. As we can see in Fig. 6 the signal-to-noise from the corrected Set A is up to ~ 15 per cent smaller at $k_{\mathrm{max}} \gtrsim 0.30\, h\,\mathrm{Mpc}^{-1}$, while at lower redshift (where the mass resolution effect is negligible) the S/N from the corrected and uncorrected Set A agree within a few percent. For comparison, we also plot the expected S/N in the Gaussian case. Assuming that the precision matrix from Set A is drawn from the inverse-Wishart distribution (Press 1982), then from the study of Taylor, Joachimi & Kitching (2013) we expect the statistical errors on S/N to be ~ 1 per cent, much smaller than the effect of mass resolution at $z > 1$. As already noted by Angulo et al. (2008), the signal-to-noise saturates above a redshift dependent scale (see also Smith 2009; Takahashi et al. 2009).

In Fig. 7 we plot the signal-to-noise at $k_{\mathrm{max}} = 0.40\, h\,\mathrm{Mpc}^{-1}$ (a scale on the plateau of the S/N) as function of the number of realisations at different redshifts. As we can see the signal-to-noise converges for $N_s > 4000$ at all the redshifts within a few per cent.

Here, it is worth noticing that the signal-to-noise has been estimated using an unbiased estimator of the precision matrix, Eq. (9). However, this is only valid in the Gaussian case for which the probability distribution of the inverse covariance is given by the inverse-Wishart distribution. As we have shown in the previous Section, at low redshift and high k the statistics of the matter
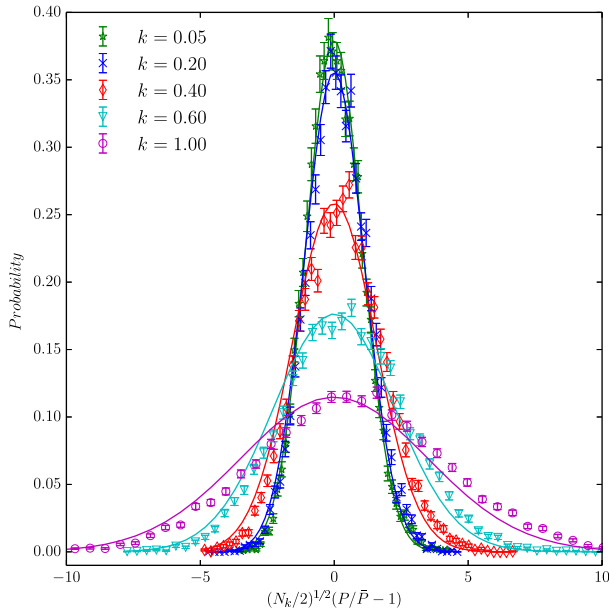
Figure 4. Probability distribution of the rescaled power spectrum estimator $\sqrt{N_k/2}(\hat{P}/\bar{P}-1)$ estimated from the 12288 realisations of Set A for $k = 0.05$ (green star) 0.20 (blue cross) 0.40 (red diamond), 0.60 (light-blue triangle) and $1.00\,h\,\mathrm{Mpc}^{-1}$ (magenta circle) respectively. The error bars are given by Poisson errors. The solid line curves show the Gaussian distribution with sample mean and variance of the same set at the corresponding values of k.

power spectrum deviates from that of Gaussian random density field. Hence, it is reasonable to expect a departure of the precision matrix from the inverse-Wishart distribution at these scales and redshifts. This is particularly relevant for cosmological model parameter estimations and studies along the line of the analysis by (Taylor, Joachimi & Kitching 2013; Taylor & Joachimi 2014) using the DEUS-PUR simulations can be particularly informative. A study which we leave to future work.

6 CONCLUSION

The covariance matrix of the matter power spectrum is an essential ingredient to infer unbiased cosmological parameter constraints from measurements of the clustering of matter in the universe. The next generation of galaxy surveys will precisely measure the matter power spectrum across a wide range of scales. This demands for an accurate estimation of the covariance matrix. Here, we have tackled this task using a large ensemble of numerical N-body simulations from the DEUS-PUR project. First, we have assessed the impact of numerical systematic uncertainties due to mass resolution effects using a reduced sample of higher resolution simulations. We have provided an empirical statistical method to correct for this source of non-Gaussian error on the covariance matrix. By taking advantage of the large statistics of the DEUS-PUR simulations we have finely sampled the power spectrum probability distribution. We have found a non-vanishing skewness which deviates from the expectations of a Gaussian density field at low redshifts ($z \leq 0.5$) with the amplitude of the deviations increasing on scales $k \gtrsim 0.25\,h\,\mathrm{Mpc}^{-1}$. The non-Gaussian errors resulting from the non-linear regime of gravitational collapse mildly affect the spec-
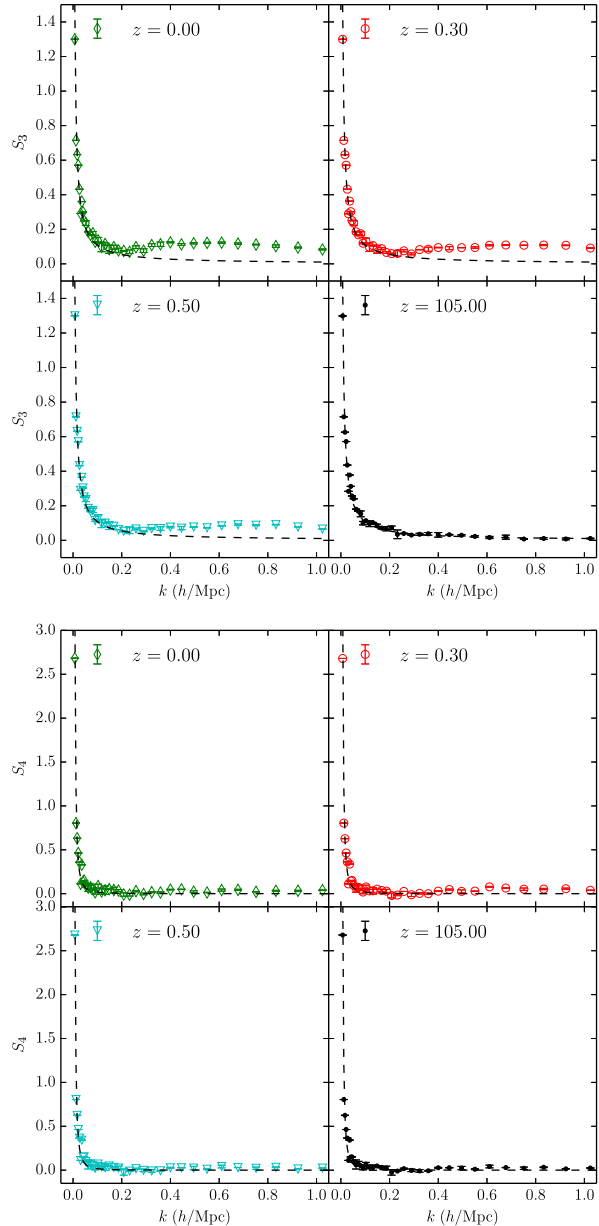

Figure 5. Skewness (top panels) and kurtosis (bottom panels) of the probability distribution of $\hat{P}$ as a function of k for $z = 0, 0.3, 0.5$ and 105 respectively. The measured values are binned in intervals of size $\Delta k/k \sim 0.1$, the associated Poisson errors are smaller than the data points. The dashed lines represent the χ^2-distribution predictions.

trum on BAO scale, in contrast they become important at smaller scales. This suggests that an unbiased estimate of the ensemble averaged band power from finite volume surveys at these scales and redshifts may require the full probability distribution of the matter power spectrum. The ensemble of N-body simulations from the DEUS-PUR project can provide a valuable support to these future analyses.
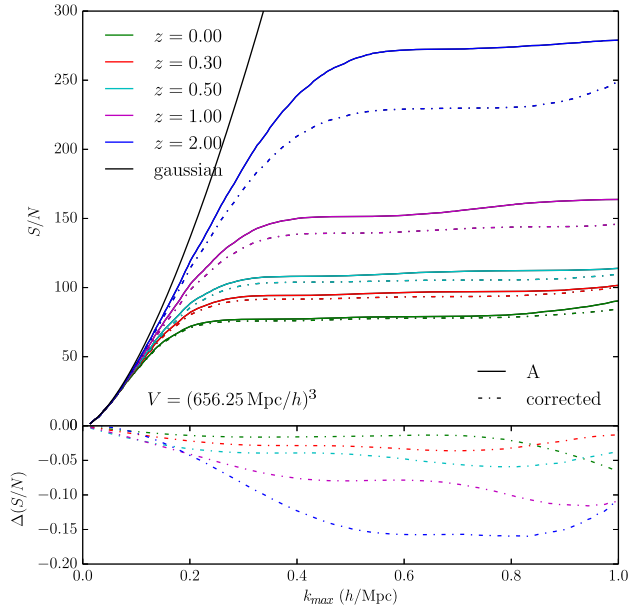
Figure 6. Top panel: signal-to-noise of power spectrum measurements as function of k_{max} estimated from Set A with (solid line) and without (dash line) mass resolution correction for $z = 0, 0.3, 0.5, 1$ and 2 respectively. The solid black line corresponds to the Gaussian prediction. Bottom panel: relative difference of the S/N with and without mass resolution correction.
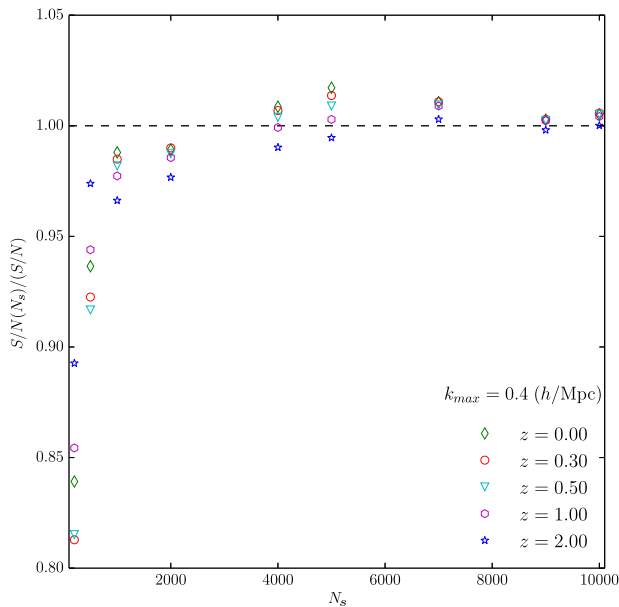

Figure 7. Signal-to-noise of power spectrum measurements at $k_{max} = 0.40\,h\,\mathrm{Mpc}^{-1}$ estimated from sub-samples of Set A with mass resolution correction and normalised to the signal-to-noise of the full Set A for $z = 0, 0.3, 0.5, 1$ and 2 respectively. Convergence at the per cent level is achieved for $N_s > 4000$.

REFERENCES

Abell, P. A. et al., 2009, arXiv:0912.0201
Alimi, J.-M. et al., 2012, IEEE Computer Soc. Press, CA, USA, SC2012, Article No 73
Amendola, L. et al., 2013, Living Rev. Relativity, 16, 6
Anderson L. et al., 2013, arXiv:1312.4877
Angulo R. et al., 2008, MNRAS, 383, 755
Angulo R. et al., 2012, MNRAS, 426, 2046
Cole S. et al., 2005, MNRAS, 362, 505
Crocce M., Pueblas S., & Scoccimarro R., 2006, MNRAS, 373, 369
Dawson K.S. et al., 2013, Astron. Journ., 145, 10
Eisenstein D.J. et al., 2005, ApJ, 633, 5
Fisher, K.B. et al., 1993, ApJ, 402, 42
Guillet T., Teyssier R., 2011, Journal of Computational Physics, 230, 4756
Hartlap J., Simon P., Schneider P., 2007, A&A, 464, 399
Heitmann, K., White, M., Wagner, C., Habib, S., & Higdon, D., 2010, ApJ, 715, 104
Joyce M., Marcos B., Bertschiger T., 2009, MNRAS, 394, 751
Kiessling A., Taylor A.N., Heavens, 2011, MNRAS, 416, 1045
Kim et al., 2011, JKAS, 44, 217
Knebe, A., Green, A., & Binney, J., 2001, MNRAS, 325, 845
Lee J., Pen U.-L., 2008, ApJ, 686, L1
Meiksin, A., White, M., 1999, MNRAS, 308, 1179
Ngan, W., Harnois-Déraps, J., Pen, U.-L., McDonald, P., & MacDonald, I., 2012, MNRAS, 419, 2949
Percival W.J. et al., 2001, MNRAS, 327, 1297
Percival W.J. et al., 2007, MNRAS, 381, 1053
Press S.J., 1982, Applied Multivariate Analysis
Prunet, S. et al., 2008, ApJs, 178, 179
Rasera Y. et al., 2014, MNRAS in press, arXiv:1311.5662
Rimes C.D., Hamilton A.J.S., 2005, MNRAS, 371, 1205
Sato M., et al., 2009, ApJ, 701, 945
Scoccimarro R., 1998, MNRAS, 299, 1097
Scoccimarro R., Zaldarriaga M., Hui L., 1999, ApJ, 527, 1
Semboloni E. et al., 2007, MNRAS, 375, L6
Skillman S. W., Warren M. S., Turk M. J., Wechsler R. H., Holz D. E., Sutter P. M., arXiv:1407.2600
Smith R.E., 2009, MNRAS, 400, 851
Spergel, D. N., et al., 2007, ApJs, 170, 377
Takahashi, R. et al., 2009, ApJ, 700, 479
Takahashi, R. et al., 2011, ApJ, 726, 7
Taylor A., Joachimi B., Kitching T., 2013, MNRAS, 432, 1928
Taylor A., Jaochimi B., 2014, arXiv:1402.6983
Tegmark M. et al., 2004, ApJ, 606, 702
Teyssier, R., 2002, A&A, 385, 337
White S., Hu W., 2002, ApJ, 537, 1

z	α	β	γ	δ
0	-0.156	0.569	-0.442	0.146
0.3	0.098	-0.039	-0.290	0.188
0.5	-0.410	0.695	-0.895	0.343
1	0.266	1.026	0.280	0.252
2	2.240	-5.272	2.924	-0.051

Table A1. Best-fitting values for the parameters α, β, γ and δ.

APPENDIX A: MASS RESOLUTION CORRECTION TO MATTER POWER SPECTRUM

Here, we derive the mass resolution correction to the matter power spectra estimated from Set A.

We assume that the corrected power spectrum estimator, $\hat{P}_A^{\mathrm{corr}}$, and that of the lower resolution simulations, $\hat{P}_A$, are related by a simple linear transformation:

$$\hat{P}_A^{\mathrm{corr}} = a\,\hat{P}_A + b. \tag{A1}$$

The goal here is to find a correction that maps each of the $\hat{P}_A$ from the pdf of Set A, $f(\hat{P}_A)$, into the one of Set B, $f(\hat{P}_B)$. Since the proposed correction has two parameters, we only need the first two moments of $f(\hat{P}_B)$ to correct the spectra of Set A. In principle one can assume higher order corrections, but then higher moments of $f(\hat{P}_B)$ are needed for the computation, and the statistics of our sample is not sufficient to resolve them.
We determine the coefficients a and b by imposing that the average $\bar{P}_A^{\mathrm{corr}} = \bar{P}_B$ and the variance $\sigma^2_{\hat{P}_A^{\mathrm{corr}}} = \sigma^2_{\hat{P}_B}$. Those conditions translate in the system:

$$\bar{P}_B = a\,\bar{P}_A + b, \tag{A2}$$

$$\sigma^2_{\hat{P}_B} = a^2\,\sigma^2_{\hat{P}_A}, \tag{A3}$$

from which we finally obtain Eq. (4):

$$\hat{P}_A^{\mathrm{corr}} = \frac{\sigma_{\hat{P}_B}}{\sigma_{\hat{P}_A}}\hat{P}_A + \bar{P}_B - \frac{\sigma_{\hat{P}_B}}{\sigma_{\hat{P}_A}}\bar{P}_A. \tag{A4}$$

The standard deviation of the power spectra from Set B is very noisy, and so is the ratio $\sigma_{\hat{P}_B}/\sigma_{\hat{P}_A}$. We find convenient to smooth out this noise and assume a fourth grade polynomial fitting function of k, such that $\sigma_{\hat{P}_B}/\sigma_{\hat{P}_A} \equiv \alpha\,k^4 + \beta\,k^3 + \gamma\,k^2 + \delta\,k + 1$ where $\alpha, \beta, \gamma, \delta$ are the fitting parameters that we obtain by fitting the polynomial function to the numerical ratio of the standard deviations. We impose that on the large linear scales, e.g. at $k_{\min}$ this ratio tends to unity since in this regime there is no difference between Set A and B.

In Fig. A1 we plot $\sigma_{\hat{P}_B}/\sigma_{\hat{P}_A}$ and the best-fitting smoothing function at $z = 0, 0.3, 0.5, 1$ and 2 respectively. The best-fitting values of the parameters are quoted in Table A1.
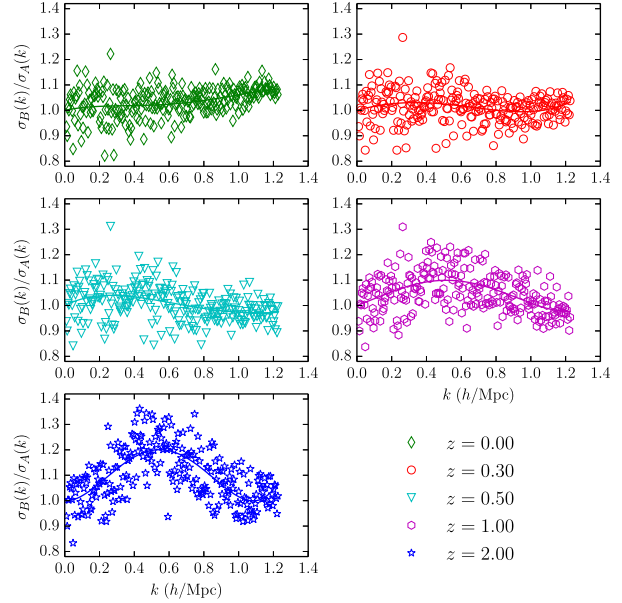

Figure A1. Ratio of the standard deviation of the spectra from Set B and A, $\sigma_{\hat{P}_B}/\sigma_{\hat{P}_A}$ as function of k at $z = 0, 0.3, 0.5, 1$ and 2 respectively. The solid lines are the best-fitting smoothing functions.